

# Theory and Models of Colliding Stellar Winds

J. M. Pittard

School of Physics and Astrophysics, University of Leeds, United Kingdom

Published in proceedings of

“Stellar Winds in Interaction”, editors T. Eversberg and J.H. Knapen.

Full proceedings volume is available on <http://www.stsci.de/pdf/arrabida.pdf>

**Abstract:** I discuss some of the important aspects of the phenomena of colliding winds in massive binary star systems with a particular focus on WR 140.

## 1 Introduction

Luminous stars are able to drive powerful winds which, while ploughing into their surroundings, may also cause significant mass loss and thus modify the star’s evolution. Determining the rate of mass loss is key to understanding how such stars evolve. Fortunately, in massive binary systems we are able to use the wind of one star as an in-situ probe of the wind of the other star. In addition, the collision of the winds unleashes a broad spectrum of emission revealing the interesting physics of high Mach number shocks, including the acceleration of a small proportion of particles to relativistic energies.

## 2 The Dynamics of Colliding Wind Binaries

### 2.1 Instabilities

The nature of the wind-wind collision in colliding wind binaries (CWBs) depends on a number of factors, and displays a huge diversity. For instance, in some systems the winds are of almost equal strength and collide roughly mid-way between the stars. In others, one wind is significantly more powerful than the other and completely overwhelms the weaker wind, causing the collision region to crash onto the surface of the companion star. Hence the nature of the wind-wind collision region (WCR) depends on the wind properties of the system. The thermal behaviour of the WCR also depends on the orbital properties of the system. In short period systems, where the two stars are very close together, the wind-wind collision is likely to be highly radiative. The shock-heated gas therefore cools very rapidly, and a geometrically thin and dense region of gas forms which is prone to severe, and perhaps disabling, non-linear thin-shell instabilities (NTSI, Vishniac 1994)<sup>1</sup>. On the

---

<sup>1</sup>This is the conventional wisdom, but in fact it is not clear exactly what occurs between the stars—e.g. even whether two “winds” are produced—in such an extreme and hostile environment.

other hand, if the orbital period is long, the shocked gas may behave largely adiabatically, flowing out of the system while still hot. In this case the WCR stays thick and “puffed-up”, and is far less affected by disruptive instabilities, although Kelvin-Helmholtz instabilities, due to a velocity shear at the contact discontinuity between the winds, may still occur. Where one wind is radiative and the other largely adiabatic, a thin dense layer of cooled gas abuts a thicker, hotter, but more rarefied layer which acts like a “cushion” to damp out thin shell instabilities occurring in the dense layer (Vishniac 1983). These differences were illustrated by Stevens et al. (1992) and are reproduced in Fig. 1.

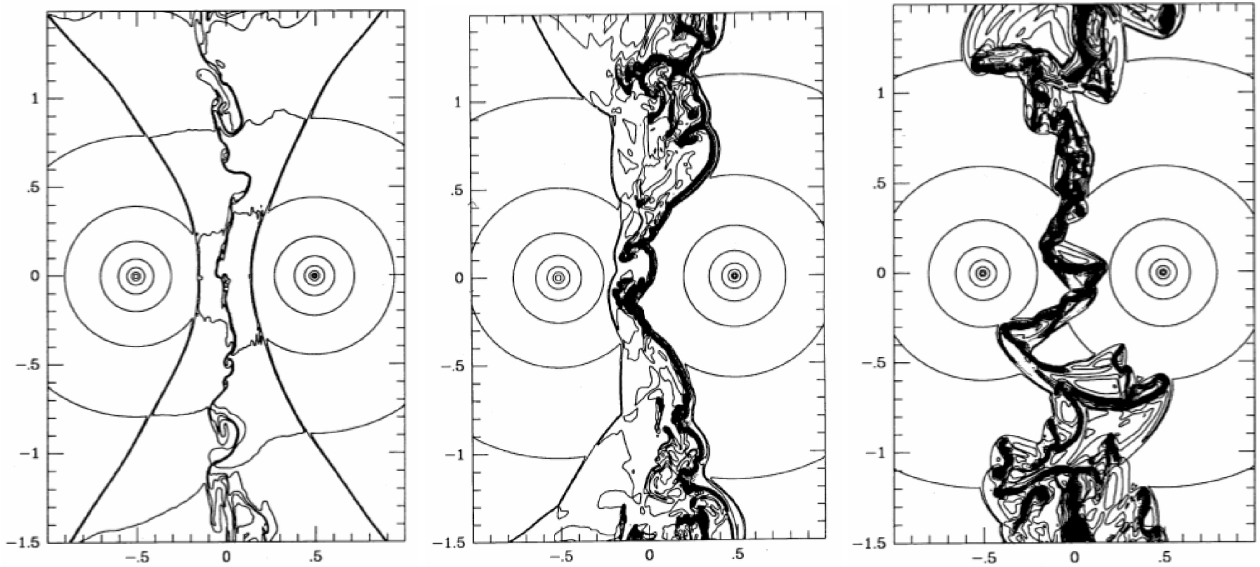


Figure 1: Instabilities in the WCR of CWBs. *Left:* When both sides of the contact discontinuity are largely adiabatic, the WCR is very smooth. *Center:* When one side is radiative, thin shell instabilities occur, but are somewhat limited by the “cushioning” of the hot gas (Vishniac 1983). *Right:* When both sides are radiative, the much stronger and highly non-linear thin shell instability occurs (Vishniac 1994). Adapted from Stevens et al. (1992).

The transition between radiative and adiabatic post-shock regions is conveniently estimated using the value of  $\chi \equiv t_{\text{cool}}/t_{\text{dyn}} \approx v_8^4 D_{12}/\dot{M}_{-7}$ , where  $t_{\text{cool}}$  is the cooling time of the gas,  $t_{\text{dyn}}$  is a dynamical flowtime which is rather loosely defined but can be taken as either the time for shocked gas at the apex of the WCR to flow a distance  $D_{\text{sep}}$  downstream, or for the shocked gas from the weaker wind to flow a distance  $r_{\text{OB}}$  downstream (see Stevens et al. 1992 for these definitions). In the above,  $v_8$  is the wind speed normalised to  $1000 \text{ km s}^{-1}$ ,  $D_{12}$  is the stellar separation normalised to  $10^{12} \text{ cm}$ , and  $\dot{M}_{-7}$  is the mass-loss rate normalised to  $10^{-7} M_{\odot} \text{ yr}^{-1}$ . Note that this formalism for  $\chi$  depends on specific assumptions about the post-shock temperature and the morphology of the cooling curve at this point (see Pittard & Stevens 2002). By specifying appropriate values for  $\dot{M}_{-7}$ , etc., it is possible to determine a separate value of  $\chi$  for each shocked wind.

One of the reasons why WR 140 is of particular interest is that its highly eccentric orbit results in big, but reproducible, changes in the properties of the WCR, for instance its density. While the shocked O-star wind is largely adiabatic throughout the entire orbit, the same is not true of the shocked WR wind, which though adiabatic at apastron ( $\chi_{\text{WR}} \sim 50$ ), has much more significant cooling at periastron ( $\chi_{\text{WR}} \sim 2$ ). At this time the shocked gas radiates away all of its energy as it leaves the system, seemingly creating the ideal conditions for dust formation (P. Williams, these proceedings). A signature of this cooling is believed to be seen in the He I  $1.083\text{-}\mu\text{m}$  line, which develops a sub-peak on top of its normal flat-topped profile as the stars approach periastron (see Varricatt, Williams & Ashok 2004, and also P. Williams, these proceedings).

The exact thermal behaviour of the shocked gas is impossible to determine without fully three-dimensional numerical simulations, since the value of  $\chi$  as estimated above is only approximate. A number of other mechanisms can also influence the value of  $\chi$ . For instance, if the winds are clumpy, which is believed to be the case for hot stars, the cooling and hence  $\chi$  will be underestimated. Furthermore, the efficient acceleration of non-thermal particles in the WCR may sap energy from the thermal plasma, again causing it to cool more rapidly. Therefore, values of  $\chi$  estimated using the above equation should be taken as only a rough guide of the true thermal behaviour.

## 2.2 Radiative Driving Effects

Systems where the stars are relatively close to each other (i.e. those with short periods and/or highly eccentric orbits) may suffer from interactions between one star's wind and the other star's radiation field. Two scenarios have been determined. In the "radiative inhibition" scenario, the acceleration of one or both winds is inhibited by the radiation field of the other star, thus reducing the speed of the wind(s) before the collision (Stevens & Pollock 1994). Another effect, termed "radiative braking" comes into play in systems where the stronger wind closely approaches the more luminous star (Gayley et al. 1997). This condition is met in many Wolf-Rayet (WR) + O-star binaries. The stronger radiation field may then efficiently couple to the more powerful wind, causing a sudden deceleration or braking. The effect is highly non-linear, and the braking can be so severe that the stronger wind can be prevented from colliding with the surface of the more luminous star even in cases where a normal ram-pressure balance between the winds would not be possible. Neither of these effects is believed to be important in WR 140, since even at periastron the stars are still well separated (see R. Fahed et al., these proceedings), and the WCR is at least several stellar radii from the surface of the O-star despite the large disparity in wind strengths.

## 2.3 Orbital Effects

The orbit of the stars can also strongly influence the properties and nature of the WCR. The most obvious effect is a spiralling of the WCR as the gas within it flows out of the system. Due to the large computational cost of 3D simulations, it is only recently that the first 3D hydrodynamical models of colliding wind binaries were presented in a refereed journal (Lemaster et al. 2007), and this work lacked several key processes which are important in the short-period systems where the effects of orbital motion are greatest. The most notable omissions were the lack of any treatment for the acceleration of the winds and the cooling of the shocked gas. Shortly afterwards, 3D smoothed-particle hydrodynamics (SPH) simulations of the WCR in the massive binary system  $\eta$  Carinae were presented (Okazaki et al. 2008). Though these models were isothermal, and did not solve for the temperature structure behind the shock, they provided much insight into the dynamics of the WCR in this highly eccentric ( $e \approx 0.9$ ) system. At about the same time, a "dynamic" model was presented by Parkin & Pittard (2008). This model did not solve the hydrodynamic equations, but instead mapped the apex of the WCR (given by the equations in Stevens et al. 1992) into a 3D space. The apex was provided with a time-dependent skew which aimed to reflect the ratio of the wind to orbital speeds, and the gas was assumed to behave ballistically further downstream. Though the resulting dynamics are only representative of the true situation, a comparison against results from a full hydrodynamical calculation revealed that this approach does a more than adequate job in many situations.

The first 3D simulations of CWBs to include orbital motion, the radiative driving of the winds and cooling of the shocked gas were presented by Pittard (2009). Focusing on O+O-star systems, models with circular orbits were presented. Depending on the orbital period (3 d or 10 d) the WCR was either highly radiative or largely adiabatic. In the former, differences in the nature of the instabilities in

the leading versus the trailing edge of each “arm” of the WCR are seen. In the latter, the density and temperature of the hot gas changes across the arms. The most interesting behaviour, however, was seen from a system with an eccentric orbit where the stellar separation at periastron was the same as the system with the 3 d orbital period, while the apastron separation was the same as the system with the 10 d orbital period - this required  $e = 0.36$ . Most notably, the properties of the WCR exhibited a distinct phase lag compared to those expected from the instantaneous position of the stars, which reflects the recent history of the stellar separation. Hence there were marked differences in the WCR properties when the stars are at identical stellar separations depending on whether the stars are approaching or receding from each other. For instance, the gas in the WCR remains hot until near phase 0.9, after which it collapses into a thin dense sheet which is torn apart by instabilities. Yet it is past apastron before the cold clumps are cleared away from the stars (this long timescale is due to the high inertia of the dense clumps relative to the rarefied gas which flows past them). This process is clearly shown in synthetic images at 1000 GHz (see Fig. 2).

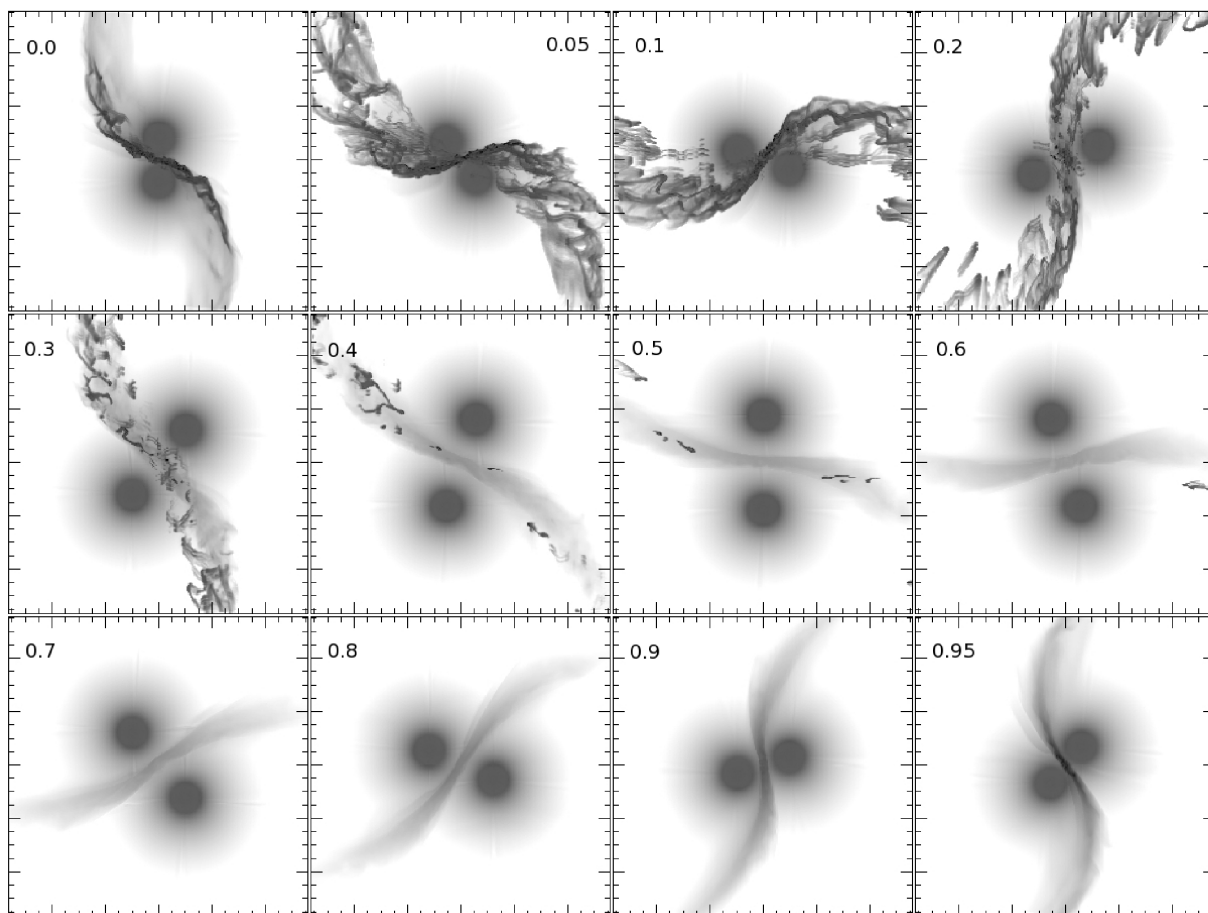


Figure 2: Intensity images at 1000 GHz for an observer viewing an eccentric ( $e = 0.36$ ) O+O-star system with an orbital period of 6.1 d (adapted from Pittard 2010). See Pittard (2009) for details of the hydrodynamical model).

For most of WR 140’s orbit, orbital effects are minimal, and the WCR is approximately axisymmetric, with rotational symmetry about the line running through the centres of the stars. However, orbital effects become very significant as the stars swoop through periastron passage. The rapid changes in the positions of the stars induces severe curvature into the WCR, breaking the axisymmetry which exists up until about phase 0.95. One must then be careful when interpreting data using axisymmetric models for the WCR (e.g. the Lührs 1997 model), since this curvature will bias estimates of the

opening angle of the WCR, and thus of the momentum ratio of the winds.

## 2.4 The Effect of Clumpy Winds

Studies of how wind clumping affects the WCR have been presented by Walder (1998), who showed that dense clumps can tip an otherwise marginally adiabatic WCR into a radiative regime. Pittard (2007) examined the effect of clumps on the adiabatic WCR of WR 140 at apastron. If the clumps are not too dense or large (so that they do not punch through the WCR), they can be rapidly destroyed by the vorticity created during their passage through the shocks bounding the WCR. Although the WCR becomes highly turbulent as a result, the overall effect is to smooth out the flow. Thus determinations of the stellar mass-loss rates using the X-ray emission from a WCR may be relatively insensitive to clumping, and thus offer a useful alternative to other methods where this is not the case. The strong turbulence occurring within the WCR also has implications for particle acceleration and the mixing of the winds.

## 3 Models of WR 140

Due to its interesting behaviour, WR 140 is one of the best studied CWB systems, and this has led to the development of a large number of theoretical models. Each model has typically addressed one aspect of its emission. In the following I summarise the models which have been made of the thermal X-ray and non-thermal radio emission. The latter have also been used to predict the expected flux of the high-energy non-thermal emission, so I will discuss these too. I will not discuss the thermal IR emission from WR 140, which has been extensively studied and modelled by Peredur Williams and collaborators, details of which are given in the contribution by Peredur Williams in these proceedings.

### 3.1 Thermal X-ray Emission

WR 140 is an exceptionally luminous X-ray source for a colliding wind binary system, with an X-ray luminosity  $\sim 4 \times 10^{34} \text{ erg s}^{-1}$ . This indicates that, in addition to the strong, dense and fast wind from the Wolf-Rayet star, the companion star must also have a powerful wind (the maximum efficiency for converting wind power into hot shocked gas is obtained when the winds are of equal strength). The X-ray luminosity displays large, phase-repeatable, variations around the orbit. Such variations must reflect the underlying changes occurring to the hot plasma in the WCR, augmented by changes in the circumstellar absorption from the surrounding winds (see, e.g., M. Corcoran et al., these proceedings).

To model the emission from the WCR with hydrodynamic codes, one must resolve the cooling length behind the shock. This is a difficult task when the cooling is very rapid, but perfectly possible for WR 140 since the shocked gas is never strongly radiative. Early predictions for the X-ray spectrum and lightcurve were made by Stevens et al. (1992). The predicted X-ray luminosity scales as  $D^{-1}$ , where  $D$  is the stellar separation, and there is a deep X-ray minimum as the orbit moves the denser wind of the WR star in front of the apex of the WCR. Prior to this work, a simple point-source model for the X-ray absorption was constructed to compare against the observed absorption of EXOSAT spectra (Williams et al. 1990). Today, observations by the *RXTE* X-ray satellite reveal the X-ray lightcurve in exquisite detail (see M. Corcoran et al., these proceedings). An immediate puzzle is that the expected  $D^{-1}$  scaling is not observed—instead the real increase is lower. This has yet to be explained, but may be related to the cooling of the plasma or the acceleration of non-thermal particles within the WCR. Furthermore, models which adopt spatially extended X-ray emission at the WCR are not able to reproduce the deep X-ray minimum (see, e.g., M. Corcoran et al., these proceedings).

Several other models have investigated various physical aspects of the high Mach number shocks found in WR 140. The heating of electrons and ions at the shocks was modelled by Zhekov & Skinner (2000) who concluded that models where the electrons were heated more slowly than the ions provided better fits to the *ASCA* X-ray data available at the time (see also Pollock et al. 2005). Another process which is likely to have a significant timescale is that of ionisation equilibrium—the initial post-shock plasma is under-ionised for its temperature, and ionisation towards equilibrium proceeds as material flows downstream from the shock and eventually out of the system. This effect is beautifully illustrated in Pollock et al. (2005), where it is seen that the FWHM of various X-ray lines increases with the ionisation potential of the species. This is the opposite trend to that expected from a plasma in collisional ionisation equilibrium (CIE), where the hottest gas and most highly ionised species occur at the apex of the WCR where the shocks are perpendicular to the oncoming winds. Pollock et al. (2005) estimates that the distance for ionisation equilibrium to be established when the stars are at apastron is about 32 AU (i.e. comparable to the orbital separation). Models of X-ray line profiles (see Henley, Stevens & Pittard 2003; Henley et al. 2005, 2008) where the plasma is assumed to be in CIE fail spectacularly when an attempt is made to fit the WR 140 data. This adds further support to the plasma being in non-equilibrium ionisation.

By constructing a number of hydrodynamical models and examining the expected X-ray emission from each, Pittard & Dougherty (2006) determined a range of possible mass-loss rates and wind momentum ratios which were consistent with the observed X-ray flux. The mass-loss rates should be accurate to  $\pm 25\%$ , with uncertainties due to the ill-determined composition of the WR wind (see Pollock et al. 2005 and Pittard & Dougherty 2006 for more details). Zhekov & Skinner (2000) derived slightly higher mass-loss rates for their adopted wind momentum ratio ( $\eta = \dot{M}_O v_O / \dot{M}_{WR} v_{WR} = 0.0353$ ) as they assumed relatively low abundances for C and O. Note that previous works have sometimes used mass-loss rates which are inconsistent with the X-ray luminosity (e.g. Dougherty et al. 2005). The values of  $\eta$  investigated by Pittard & Dougherty (2006) spanned the range 0.02 – 0.2. Larger values of  $\eta$  require relatively smaller values of  $\dot{M}_{WR}$  and larger values of  $\dot{M}_O$ . The latest investigation on the sudden increase in the absorption component of the He I 1.083- $\mu\text{m}$  line near periastron implies that  $\eta = 0.1$  (see the contribution by Peredur Williams in these proceedings), which in turn implies that  $\dot{M}_{WR} \approx 2 \times 10^{-5} M_\odot \text{yr}^{-1}$  and  $\dot{M}_O \approx 2 \times 10^{-6} M_\odot \text{yr}^{-1}$ . Further (3D) modelling is needed to test these values.

### 3.2 Non-Thermal Radio Emission

In the late 1970s and early 1980s the radio emission from WR 140 was determined to be highly variable, with both the flux and the spectral index undergoing significant changes. Over the intervening years further observations in the radio have revealed in exquisite detail phase repeatable light curves and images of the emission from the WCR (see Williams et al. 1990; White & Becker 1995; Dougherty et al. 2005; S. Dougherty et al., these proceedings). Part of the modulation is thought to be caused by the variable circumstellar extinction to the source of the non-thermal (synchrotron) emission (the WCR) as the O-star orbits in and out of the radio photosphere in the dense WR wind. However, the intrinsic non-thermal emission probably also varies around the orbit. Various aspects of the particle acceleration in and non-thermal emission from CWBs were discussed by Eichler & Usov (1993).

Early models of the non-thermal radio emission from CWBs were very simple. It was usually assumed that the observed flux ( $S_\nu^{\text{obs}}$ ) was a combination of the free-free flux from the spherically symmetric winds ( $S_\nu^{\text{ff}}$ ), plus the flux from a point-like non-thermal source located at the stagnation point of the WCR ( $S_\nu^{\text{nt}}$ ). In this model the non-thermal emission is then attenuated by free-free

absorption (opacity  $\tau_{\nu}^{\text{ff}}$ ) through the surrounding winds:

$$S_{\nu}^{\text{obs}} = S_{\nu}^{\text{ff}} + S_{\nu}^{\text{nt}} e^{-\tau_{\nu}^{\text{ff}}}. \quad (1)$$

While this approach allows simple solutions to the radiative transfer equation (e.g., Williams et al. 1990; Chapman et al. 1999), such models fail to reproduce the spectral variation of the emission with orbital phase. Williams et al. (1990) therefore proposed that in future models of WR 140 the low-opacity “hole” in the dense WR wind created by the O-star’s wind should be accounted for. However, White & Becker (1995) pointed out that in WR 140, even the O-star’s wind has significant opacity. Together, these works demonstrated the need for more realistic models which account for the spatial extent of the emission and absorption from the circumstellar envelope and the WCR. More realistic models should also account for the effects of various cooling mechanisms (e.g. inverse Compton, adiabatic, etc.) on the non-thermal electron distribution, and also additional absorption mechanisms (e.g., the Razin effect).

The modelling of the non-thermal radio emission from CWBs took a dramatic jump forward when key assumptions in previous models, such as a point-like source of non-thermal emission, and a spherically symmetric, single temperature, surrounding envelope, were removed. This was achieved in Dougherty et al. (2003), where models of the thermal and non-thermal radio emission used 2D, cylindrically symmetric, hydrodynamical simulations, to more accurately describe the density and temperature structure of the system. Sight-lines to the observer could now pass through regions of both high and low opacity. The assumption of a point-source of non-thermal emission was also removed, by treating the emission in a phenomenological way where the local density of non-thermal electrons and the magnetic field strength were related to the local thermal energy density within the WCR. The non-thermal electrons were further assumed to have a power-law distribution,  $N(\gamma)d\gamma = C\gamma^{-p}d\gamma$ , where  $\gamma$  is the Lorentz factor,  $C$  is a proportionality constant which fixes the normalisation, and it was assumed that  $p = 2$  (suitable for test particle diffusive shock acceleration, with strong shocks and an adiabatic index equal to  $5/3$ ).

Although this work was not directly applied to WR 140, the results provided a great deal of new insight into the nature of the radio emission from CWBs. An immediate realisation was the potential importance of the Razin effect in attenuating the low frequency synchrotron emission within the WCR. Several key scaling relationships were also established. For instance, in the absence of IC cooling the total synchrotron emission from the entire WCR in adiabatic systems was found to scale as  $D^{-1/2}\nu^{-1/2}$  (as a reminder the X-ray emission in the optically thin, adiabatic limit, scales as  $D^{-1}$ ). In a successive paper, Pittard et al. (2006) investigated the effect of inverse Compton (IC) cooling of the non-thermal electrons as they flowed downstream from their accelerating shocks and out of the system. This work showed that with IC cooling the *intrinsic* luminosity actually *declines* with stellar separation. The effect of the stellar separation on the *thermal* radio flux was also explored. It was discovered that the *thermal* radio emission from the WCR scales as  $D^{-1}$ , in an identical way to the thermal X-ray emission. Since this emission is optically thin in systems with an adiabatic WCR, it can mimic a synchrotron component, so that one should rather cautiously interpret data with a spectral index  $-0.1 \lesssim \alpha \lesssim 0.5$  (Pittard et al. 2006).

The model of Pittard et al. (2006) was applied to WR 140 in Pittard & Dougherty (2006). Fits were obtained to data at orbital phase 0.837, which is around the peak of the non-thermal radio lightcurve. It was found that the low frequency turn-down in the radio spectrum could be explained as either free-free absorption through the surrounding stellar winds, or the Razin effect (see Fig. 3). In the former case it proved impossible to obtain a good fit to the data with  $p = 2$ . The best fit was obtained with  $p = 1.4$ , though changes to the assumed magnetic field strength allow some small variation in this value. Such indices can result from the shock re-acceleration process, whereby the non-thermal particles pass through a sequence of shocks (Pope & Melrose 1994), or from 2nd order Fermi acceleration.

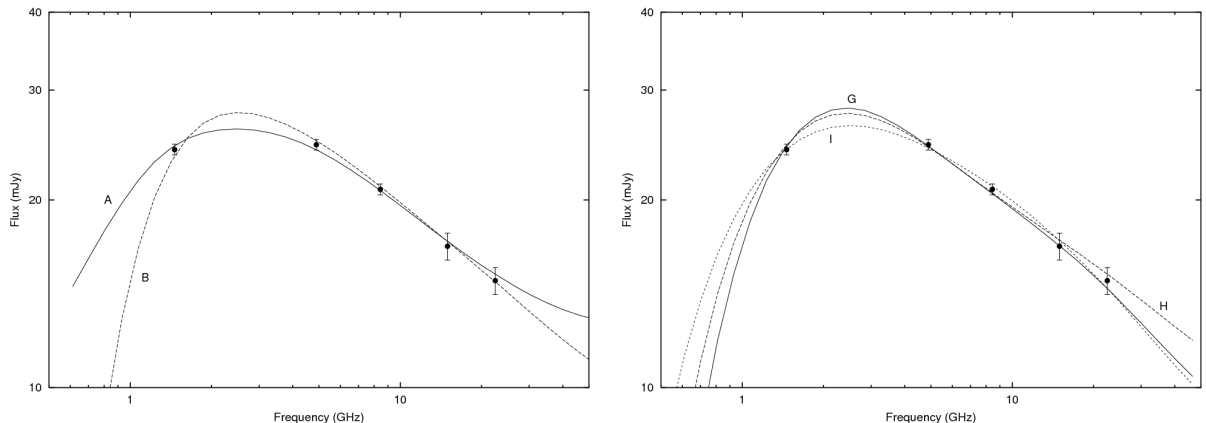


Figure 3: Model fits to the radio data of WR 140 at  $\phi = 0.837$ . *Left*: Fits where the low-frequency turn-down is due to free-free absorption. Models A and B span plausible values of the wind momentum ratio,  $\eta$ . *Right*: Fits where the Razin effect is responsible for the turn-down. For further details of the models see Pittard & Dougherty (2006).

Either of these processes may be significant in CWBs, since the clumpy nature of the winds means that the WCR is likely to be highly turbulent, with weak shocks distributed throughout it (Pittard 2007). In contrast, fits with the Razin effect dominant do allow  $p = 2$ , though require a worryingly high efficiency of electron acceleration. For this reason, fits with free-free absorption dominant were preferred. A wide range of wind momenta could fit the data in this case, though it might be possible to constrain the models with future, high sensitivity VLBA observations.

### 3.3 Non-Thermal X-ray and $\gamma$ -ray Emission

The presence of non-thermal electrons and ions should produce non-thermal emission at X-ray and  $\gamma$ -ray energies via several mechanisms, including the up-scattering of lower energy (e.g., stellar UV) photons (inverse Compton [IC] scattering), relativistic bremsstrahlung, and pion decay. Early predictions for the high-energy non-thermal emission from CWBs were made by Benaglia & Romero (2003). In this work it was assumed that IC scattering was the dominant mechanism. Then the ratio of the luminosity from IC scattering to the synchrotron luminosity is equal to the ratio of the energy density of the target photons,  $U_{\text{ph}}$ , to the magnetic field energy density,  $U_{\text{B}}$ :

$$\frac{L_{\text{ic}}}{L_{\text{sync}}} = \frac{U_{\text{ph}}}{U_{\text{B}}}. \quad (2)$$

While very straightforward, the predictive power of this equation is severely curtailed by the fact that the magnetic field strength in the WCR is generally very uncertain. Since  $U_{\text{B}} \propto B^2$ , small changes in the estimated value of  $B$  lead to large changes in  $L_{\text{ic}}$ .

In recent years the dramatic sensitivity gains achieved by space-based satellites and ground-based arrays of Cerenkov telescopes have raised the tantalising prospect of the first detection of the non-thermal X-ray and  $\gamma$ -ray emission from CWBs (in fact, we now believe that we have detected the massive CWB  $\eta$  Carinae at  $\gamma$ -ray energies, Abdo et al. 2010; Walter et al. 2010). This, in turn, has led to new theoretical predictions (e.g., Bednarek 2005). The anisotropic nature of the IC process, where the emitted power is dependent on the scattering angle, was considered by Reimer, Pohl & Reimer (2006). This work developed a two-zone model of the non-thermal emission. Particles are accelerated in an inner zone where their spatial diffusion exceeds their motion due to advection with the background fluid. Their energy distribution is self-consistently computed by considering all relevant gain



and loss mechanisms. Particles are assumed to be resident within this region until their timescales for advection and diffusion are comparable, after which they are assumed to move into the advection region where they suffer further losses as they flow downstream. Fig. 4 shows the assumed geometry and the resultant non-thermal energy spectra of the electrons and nucleons. The left panel of Fig. 5 shows the predicted IC emission from WR 140 as a function of orbital phase. While Reimer et al. (2006) conclude that while WR 140 should be easily detected with GLAST/Fermi, the high galactic background has meant that unfortunately no detection has yet been made. The change in the IC flux with viewing angle due to anisotropic scattering is likely to be obscured by large variations in the energy density of the stellar radiation fields resulting from the high orbital eccentricity.

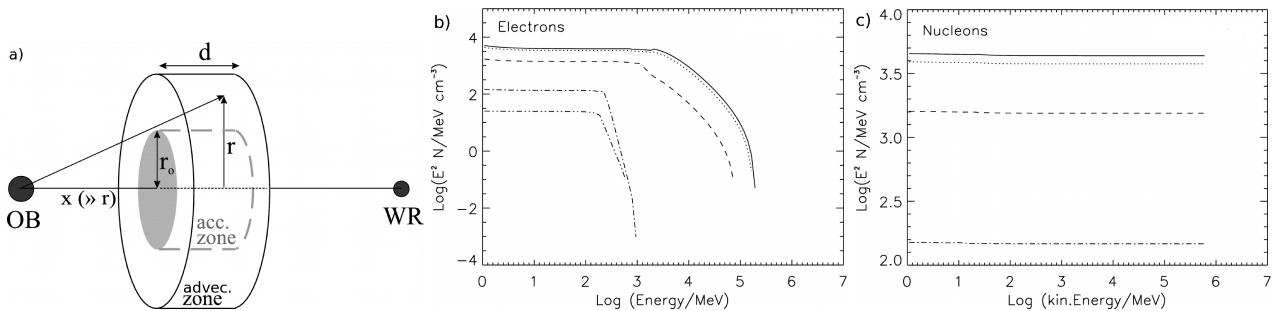


Figure 4: a) Geometry of the 2-zone model in Reimer et al. (2006). b) Evolution of the non-thermal electron spectrum from the inner acceleration zone (*solid line*) as a function of downstream distance in the advection zone. At low energies adiabatic/expansion losses dominate, while at high energies IC losses dominate. c) As b) but for nucleons. Only adiabatic losses occur. See Reimer et al. (2006) for further details.

Pittard & Dougherty (2006) also predicted the non-thermal X-ray and  $\gamma$ -ray emission from WR 140, using fits to the radio and thermal X-ray emission as constraints. The adopted approach was quite different but complementary to that of Reimer et al. (2006)—while the non-thermal particle spectrum was assumed rather than calculated, and the IC scattering was treated as isotropic, it benefitted from a more realistic description of the density and temperature distribution within the system based on the X-ray constraints. Pittard & Dougherty showed that the uncertain particle acceleration efficiency and spectral index have at least as much influence on the predicted flux as the angle-dependence of the IC emission.

The right panel of Fig. 5 shows a predicted spectral energy distribution for WR 140 from one of the models presented in Pittard & Dougherty (2006). Large differences in the predicted  $\gamma$ -ray emission occur depending on whether the low frequency turnover in the radio spectrum results from free-free absorption through the surrounding stellar winds, or from the Razin effect. While Pittard & Dougherty (2006) could not determine the nature of the absorption process from the fits to the radio spectrum, future  $\gamma$ -ray detections will determine the  $\gamma$ -ray flux and spectral index, and thus will also distinguish the nature of the low-frequency turnover. The acceleration efficiency of the non-thermal electrons and the strength of the magnetic field will then both be revealed.

## 4 Conclusions

Theoretical models of the hydrodynamics of and emission from CWBs, including of WR 140, continue to improve. Hydrodynamical models are becoming more sophisticated, with the first 3D simulations to be published in refereed journals being made in only the last several years. The goal now is to gradually add further important physics, such as non-equilibrium ionisation and electron heating,

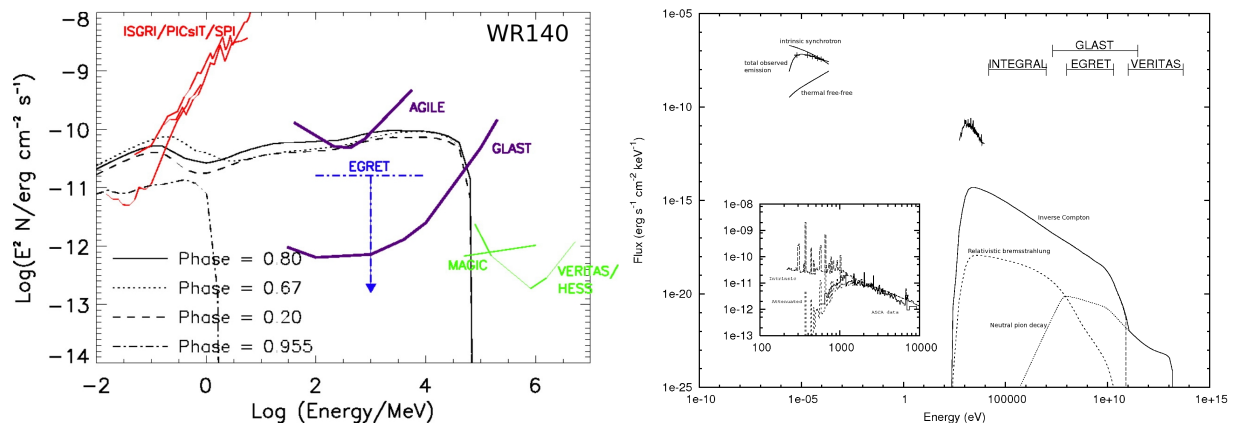


Figure 5: *Left:* Predicted IC spectra for WR 140 at phases 0.2, 0.67, 0.8 and 0.955 from Reimer et al. (2006).  $\gamma$ -ray absorption is not included. *Right:* The radio and non-thermal UV, X-ray and  $\gamma$ -ray emission calculated from model B in Pittard & Dougherty (2006), together with the observed radio and X-ray flux (both at orbital phase 0.837). The model IC (*long dash*), relativistic bremsstrahlung (*short dash*), and neutral pion decay (*dotted*) emission components are shown, along with the total emission (*solid*). See Pittard & Dougherty (2006) for more details.

to these 3D models. Predictions for the non-thermal emission have also progressed, leaving behind some of the assumptions in earlier works. Further progress will be made when the non-thermal particle distribution function is self-consistently solved with an accurate description of the post-shock flow and cooling.

## Acknowledgements

I would like to express my gratitude to the workshop organisers and to the amazing observational programme performed by the amateur astronomers. This work is supported by a University Research Fellowship from the Royal Society, UK.

## References

- Abdo A. A., et al., 2010, arXiv:1008.3235  
 Bednarek W., 2005, MNRAS, 363, L46  
 Benaglia P., Romero G. E., 2003, A&A, 399, 1121  
 Chapman J. M., Leitherer C., Koribalski B., Bouter R., Storey M., 1999, ApJ, 518, 890  
 Dougherty S. M., Beasley A. J., Claussen M. J., Zauderer B. A., Bolingbroke N. J., 2005, ApJ, 623, 447  
 Dougherty S. M., Pittard J. M., Kasian L., Coker R. F., Williams P. M., Lloyd H. M., 2003, A&A, 409, 217  
 Gayley K. G., Owocki S. P., Cranmer S. R., 1997, ApJ, 475, 786  
 Henley D. B., Corcoran M. F., Pittard J. M., Stevens I. R., Hamaguchi K., Gull T. R., 2008, ApJ, 680, 705  
 Henley D. B., Stevens I. R., Pittard J. M., 2003, MNRAS, 346, 773  
 Henley D. B., Stevens I. R., Pittard J. M., 2005, MNRAS, 356, 1308  
 Lemaster M. N., Stone J. M., Gardiner T. A., 2007, ApJ, 662, 582  
 Lührs S., 1997, PASP, 109, 504  
 Okazaki A. T., Owocki S. P., Russell C. M. P., Corcoran M. F., 2008, MNRAS, 388, L39  
 Parkin E. R., Pittard J. M., 2008, MNRAS, 388, 1047  
 Pittard J. M., 2007, ApJ, 660, L141  
 Pittard J. M., 2009, MNRAS, 396, 1743  
 Pittard J. M., 2010, MNRAS, 403, 1633

Pittard J. M., Dougherty S. M., 2006, MNRAS, 372, 801  
Pittard J. M., Dougherty S. M., Coker R. F., O'Connor E., Bolingbroke N. J., 2006, A&A, 446, 1001  
Pittard J. M., Stevens I. R., 2002, A&A, 388, L20  
Pollock A. M. T., Corcoran M. F., Stevens I. R., Williams P. M., 2005, ApJ, 629, 482  
Pope M. H., Melrose D. B., 1994, PASA, 11, 175  
Reimer A., Pohl M., Reimer O., 2006, ApJ, 644, 1118  
Stevens I. R., Blondin J. M., Pollock A. M. T., 1992, ApJ, 386, 265  
Stevens I. R., Pollock A. M. T., 1994, MNRAS, 269, 226  
Varicatt W. P., Williams P. M., Ashok N., 2004, MNRAS, 351, 1307  
Vishniac E. T., 1983, ApJ, 274, 152  
Vishniac E. T., 1994, ApJ, 428, 186  
Walder R., 1998, Ap&SS, 260, 243  
Walter R., Farnier C., Leyder J.-C., 2010, arXiv:1008.2533  
White R. L., Becker R. H., 1995, ApJ, 451, 352  
Williams P. M., van der Hucht K. A., Pollock A. M. T., Florkowski D. R., van der Woerd H., Wamsteker W. M.,  
1990, MNRAS, 243, 662  
Zhekov S. A., Skinner S. L., 2000, ApJ, 538, 808